World Electric Vehicle Journal

Article

Investigation of the Liquid Cooling and Heating of a Lithium-Ion Battery Package for an Electric Vehicle

Di Wang [1,*] and Jinhong Xie [2]

[1] Department of Mechanical Engineering, Xinjiang University, Urumqi 830046, China
[2] Guangdong Technician College of Light Industry, Guangzhou 510315, China; samdyonline@126.com
* Correspondence: wangdi1210@126.com

Abstract: The temperature of an electric vehicle battery system influences its performance and usage life. In order to prolong the lifecycle of power batteries and improve the safety of electric vehicles, this paper designs a liquid cooling and heating device for the battery package. On the device designed, we carry out liquid cooling experiments and preheating experiments. Then, a three-dimensional numerical model for the battery package is built, and its effectiveness is validated by comparing the simulation results with the experimental outcomes in terms of battery surface temperature and temperature difference. Furthermore, we investigate the influences of the liquid flow rate and the inlet temperature on the maximum temperature and temperature difference of batteries by the cooling models and preheating models. Results show that: at the cooling stage, it is able to keep each battery working at an optimal temperature under different discharge conditions by changing the flow and the inlet temperature of liquid; at the heating stage, large flow rates and high inlet temperatures are able to speed up the preheating process, thereby saving time of the drivers.

Keywords: electric vehicle; lithium-ion battery; cooling plate; cooling and heating; FEM

Citation: Wang, D.; Xie, J. Investigation of the Liquid Cooling and Heating of a Lithium-Ion Battery Package for an Electric Vehicle. *World Electr. Veh. J.* **2023**, *14*, 169. https://doi.org/10.3390/wevj14070169

Academic Editor: Ghanim A. Putrus

Received: 20 May 2023
Revised: 15 June 2023
Accepted: 21 June 2023
Published: 26 June 2023

1. Introduction

Increasingly, various electric vehicles (EVs), e.g., the Tesla Roadster and BYDE6, have been introduced because of the growing energy shortage and environmental pollution. In order to provide enough voltage and capacity for electric vehicles, lithium-ion batteries are commonly used, and hundreds of batteries are usually connected to large battery packages in series or parallel. Because electrochemical reaction produces lots of heat, the performance and usage life of lithium-ion batteries are closely related to their temperatures. According to the Arrhenius law, a high battery temperature significantly accelerates the reaction rate, resulting in a fast-aging rate [1–3]. As a result, batteries with higher temperatures degrade more quickly than the ones with lower temperatures. Obviously, the batteries should be reliable and durable enough to gain popularity.

In order to popularize EVs, one needs to ensure that EVs are able to work over a wide temperature range. Normally, the battery system can work effectively under an ambient temperature ranging from 0 °C to 32 °C. The system remains to be operational when the temperature range is extended from −25 °C to 52 °C, which may also be possible when the maximum and minimum temperature limits are, respectively, set to −40 °C and 55 °C. However, the charge efficiency and lifecycle will be reduced when the working ambient temperature is too high or too low [4–6].

Chiu et al. [7] reported that: the capacity of the battery decayed by 17% with a lifecycle of 1322 cycles when it was working with a charge/discharge rate of 0.5 C under an ambient temperature of 45 °C; however, the capacity decreased by 20% with a lifecycle of 754 cycles when it is working at a temperature of 60 °C. When the temperature of a battery rises to 70–120 °C, the phenomenon of thermal runaways such as firing and explosion may happen, which is usually triggered by the temperature rise in a single battery, thereby resulting in the degradation and failure of batteries and serious consequences [8]. Thus, it is important to involve the functions of heat dissipation and heat generation for a battery system to guarantee EVs operate well under the condition of all-weather [9].

As stated above, it is crucial to design an effective BTMS with good thermal stability and safety so as to keep each battery working at an optimal temperature range [10,11]. Besides, the thermal uniformity of each battery is also very important, because a large temperature gradient may lead to different aging levels and charge/discharge behaviors. In the BTMS, the discharge performance and lifecycle are achieved to be the best state by controlling the temperature of each battery. For a lithium-ion battery, the working temperature should not exceed 50 °C [12,13], and it is best to keep it working in a temperature range of 25 °C and 40 °C with a temperature gradient of less than 5 °C [14–16]. Because the power of a BTMS directly comes from batteries, which reduces the output power of batteries to the vehicle, the power for the BTMS should be as low as possible [17].

In recent decades, researchers have conducted large amounts of investigations on the BTMS [18–20], including the selection of cooling medium, the design of cooling systems, and the evaluation of cooling performance. With respect to the cooling medium, air, liquid, phase change material (PCM), and heat pipe are usually used. Besides, two or more cooling media can be used in one BTMS to improve cooling performance. Among the cooling methods above, air cooling can be passive/active, parallel/series, or natural/forced, which seems to be a better choice for hybrid electric vehicles (HEVs) due to its low cost, simple structure, and easy maintenance. Wang et al. [21] evaluated the air-cooling performance of a battery package with different installation positions of fans by using Fluent. Simulation results showed that it was better to install the fans above the battery package. Actually, uneven temperature distribution exists in batteries even by using forced air cooling, especially for large-scale battery packages in EVs [22]. Regarding the PCM-based BTMS, it is obviously energy-saving, because no additional power is needed from batteries. However, the thermal conductivity of paraffin is low, thus resulting in different melting rates between the surface and core of the PCM. In order to remedy this shortcoming, Khateeb et al. [23] and Mills et al. [24] added foamed aluminum and expanded graphite to PCM, respectively. One more weak point is its insufficient long-term thermal stability [25]. In [26], the cooling performance of tube heat pipes, which used water to take away the heat in the condenser, was experimentally investigated. It was found that uniform heat distribution could be guaranteed under variable power and periodic conditions, and the maximum battery temperature was lower than 50 °C when the heat generation rate was lower than 50 W. Wang et al. [27] experimentally investigated the heating and cooling performance of a battery by heat pipes. They found that the battery surface temperature was controlled to be lower than 40 °C by using the proposed scheme if the heat generated by each cell was less than 10 W. Moreover, the battery surface temperature could be down to 70 °C under thermal abuse conditions (e.g., 40 W/cell). Good preheating effectiveness was observed when the battery was preheated by using warm water in the heat pipes at a temperature range of −15 °C and −20 °C. For the two thermal management solutions by using heat pipes, an expensive metal, copper, is usually used as a wick and wall material, whose fabrication process is complicated. Besides, some other additional equipment, e.g., pumps and heat exchangers, are needed, thereby increasing power consumption.

Due to the fact that fluids are able to transfer heat faster than other substances, researchers suggest that a liquid coolant system might have stronger heat-transfer capabilities [28,29]. As the most crucial research variable, the coolant flow rate is often used as a factor by scholars in the investigation of liquid cooling systems. Kim et al. [30] used three media, i.e., the air, the oil, and the mixture of water and ethylene glycol, to investigate the heat dissipation performance of a rounded battery. They found that the performance of the mixture of water and ethylene glycol was better than that of the oil for the indirect liquid cooling systems. Furthermore, the researchers take into account not only the flux of coolant, but also the structures of the cooling board. Such as Anthony et al. [31] used water and ethylene glycol as the cooling medium for the application of interest here. In the simulations, they assumed that the heat generated by batteries was uniformly distributed, and applied the same boundary conditions to the cooling plates, then optimized the cooling plate by using the computational fluid dynamics (CFD) method. Simulation results showed that the requirements in terms of the pressure drop, and the minimum average temperature were satisfied after the optimizations of pipeline shape and position; however, the temperature uniformity was bad. CFD is often used to simulate the liquid cooling process of batteries due to its advantages in computational accuracy [32–34]. Falcone et al. [33] simulated the BTMS's heat behaviors using the CFD method. The results indicate that the application of a substance with an additive in a solid structure improves the cooled properties of the system and provides a lower temperature for the cells. A CFD model was constructed to study the influence of the input volume, the volume of the coolant pipe and the mini passage, the volume of the pipe, the direction of the flow, and the spacing between the spacers on the heat properties of the mini passage [35].

Though there is a large body of literature that reports liquid cooling for batteries [30,31], little literature involves liquid cooling for the dynamic thermal management and control strategies of battery packages. Additionally, previous literature that reports the liquid preheating of batteries is rare. In this paper, experimental investigations and numerical simulations are carried out to analyze the relationships between the thermal performance (i.e., cooling and the preheating rate) and inlet variables (i.e., inlet temperature and flow) of a battery package by using the mixture of water and ethylene glycol as the cooling medium under different conditions (e.g., different ambient temperatures and discharge rates), so as to provide a reference for the dynamic thermal management and control strategies of battery packages.

Compared with the existing research, the innovation and contribution of this paper are as follows:

(1) A liquid cooling and heating device for the battery package was developed and used to study the liquid cooling and preheating process of the cell experimentally;
(2) A three-dimensional numerical model was built, whose effectiveness was validated by comparing the simulation results with the corresponding experimental outcomes;
(3) On the numerical model, we investigated the influences of the liquid flow rate and the inlet temperature on the maximum temperature and temperature difference of batteries.

2. Liquid Cooling Experiment

2.1. Discharge Process of a Single Battery

In order to investigate the influence of the temperature on the discharge performance of a battery to obtain the rise temperatures of a single battery under different conditions, five thermocouple temperature sensors are deployed at the five points of the battery surface, as shown in Figure 1a. During experiments, the single battery is wrapped by an insulted foam coating so as to model an adiabatic condition, as shown in Figure 1b. Table 1 shows the thermal physical parameters of a 10 Ah lithium-ion battery.

Table 1. Thermal physical parameters of the 10 Ah lithium-ion battery.

Battery Component	Constituent	Density ρ (kg/m^3)	Specific Heat Capacity J/(kg·K)	Thermal Conductivity Coefficient W/(mK)
Electric core	Au, Al, Graphite, LiFeCoPO4	1958.7	733	x = 0.9; y, z = 2.7
Positive pole	Al	2713	903	238
Negative pole	Au	8900	385	385
Air gap	air	1.225	1006.43	0.0242
Shell	Al	2713	903	238

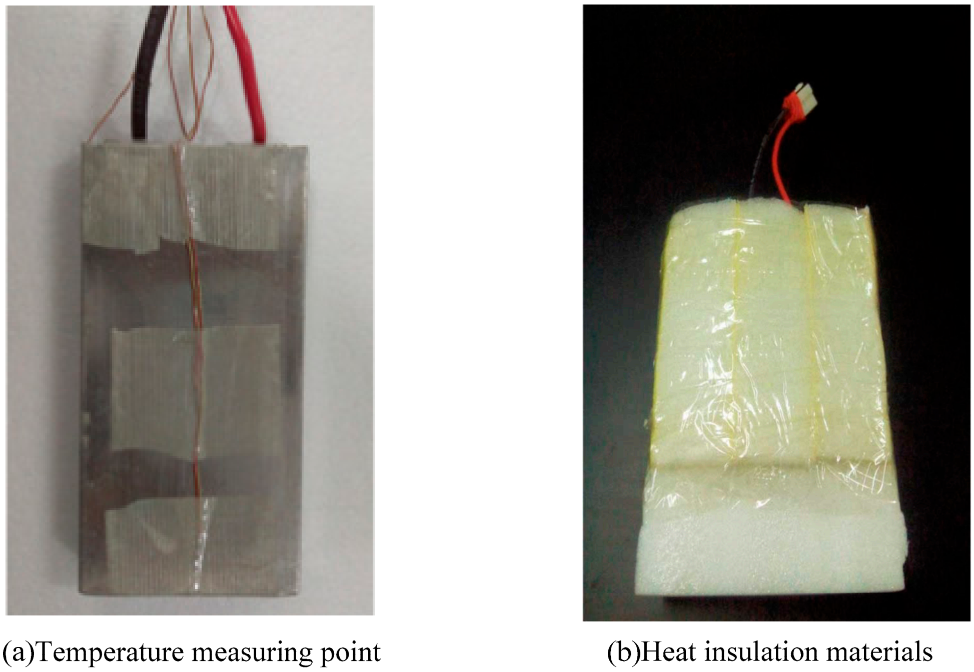

Figure 1. The temperature measuring points and the thermal insulation for the battery.

Firstly, the battery is charged at a constant current of 3 A (0.3 C) to 3.65 V; then, it is charged at a constant voltage of 3.7 V to 0.5 A (0.05 C). After charging, it is placed in a thermal chamber at a temperature of 25 °C for 3 h. Afterward, the battery is discharged at 1 C (10 A), 2 C (20 A), 3 C (30 A), and 4 C (40 A) rates down to 2.5 V, respectively, as shown in Figure 2.

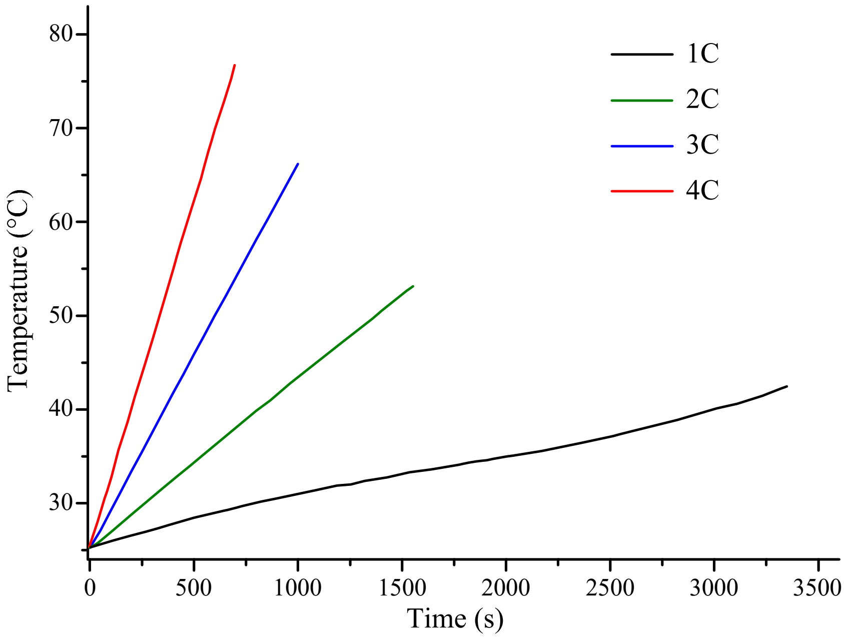

Figure 2. The average temperature versus time curves of the battery at constant currents of 10 A, 20 A, 30 A, and 40 A.

Remark 1. *Once the cell has been charged, the temperature is inconsistent on the surface. We keep the charged battery in the thermal chamber for a prolonged period of time, for example, three hours, so as to make sure that all the points of the cell are identical, and then we can study the discharge procedure of the cell with a uniform initial temperature.*

The calorific value calculation formula can be written as follows:

$$Q = c_p m \Delta T \tag{1}$$

where Q is the calorific value; c_p is the specific heat capacity; m denotes the quality; ΔT means the temperature rising.

By introducing Equation (1) into the thermal power calculation formula, we can obtain the following:

$$P = \frac{c_p m \Delta T}{t} \tag{2}$$

where P is the thermal power, and t denotes the time.

From Figure 2, we can see that: the battery surface temperature increases along with the rise of the discharge rate in the case with an environment temperature of 25 °C. The larger the discharge rate, the higher the battery surface temperature after charging, which are 42.39 °C, 53.84 °C, 66.19 °C and 76.65 °C with the discharge rates of 1 C (10 A), 2 C (20 A), 3 C (30 A) and 4 C (40 A), respectively in Table 2. When the battery is discharged at a high discharge rate, its discharge performance deteriorates due to the long-term high temperature. Consequently, it is of vital importance to investigate the thermal effect of the battery so as to improve its discharge ability at a high discharge rate.

Table 2. The battery is discharged with the rising temperature at constant current rates of 1 C, 2 C, 3C, and 4 C.

Discharge Rate	Temperature Rise (°C)	Time (s)
1 C	18.29	3350
2 C	28.84	1550
3 C	41.19	948
4 C	51.65	675

2.2. Cooling Experiment

In this paper, a liquid cooling system is designed for the battery package. The system consists of a cooling board, a heat-sensitive silicon board, a rubber pipe, a flowmeter, regulating valve, and a thermal camera. The flow of fluid inside the equipment can be determined through the flowmeter and set to be a constant value by the regulating valve. The cooling plate consists of a substrate and a lid. The substrate has a thickness of 2.5 mm and a lid of 0.5 mm [32]. The cooling tube is arranged on the bottom board, and a fluid tube is arranged at the entrance and exit of the cooling board. The silicon heating sheet is glued to the side of the cooling plate, which is used as a heater. During the experiment, we set the power of the heater at 5 W and the flow at 0.001 kg/s.

Figure 3 shows the structure of the test platform, including a battery comprehensive performance tester (Digatron BNT 200-100 ME) and a thermal chamber. The voltage and current ranges of the battery comprehensive performance tester are 0–100 V and 0–200 A, respectively.

The voltage and the capacity of a single battery are relatively small; thus, large numbers of batteries are usually connected in series to be the power source of an EV. However, these batteries might suffer from minor differences in voltage, capacity, and internal resistance because of the possible nonuniformity in manufacturing and materials. Meanwhile, the heat production rate of each battery is also influenced by the differences in charge and discharge degrees, ambient temperatures, and heat dissipation conditions. As a result, a consistency test needs to be carried out for each battery before being connected to a package, so as to guarantee good consistency for a battery package under different charge and discharge conditions.

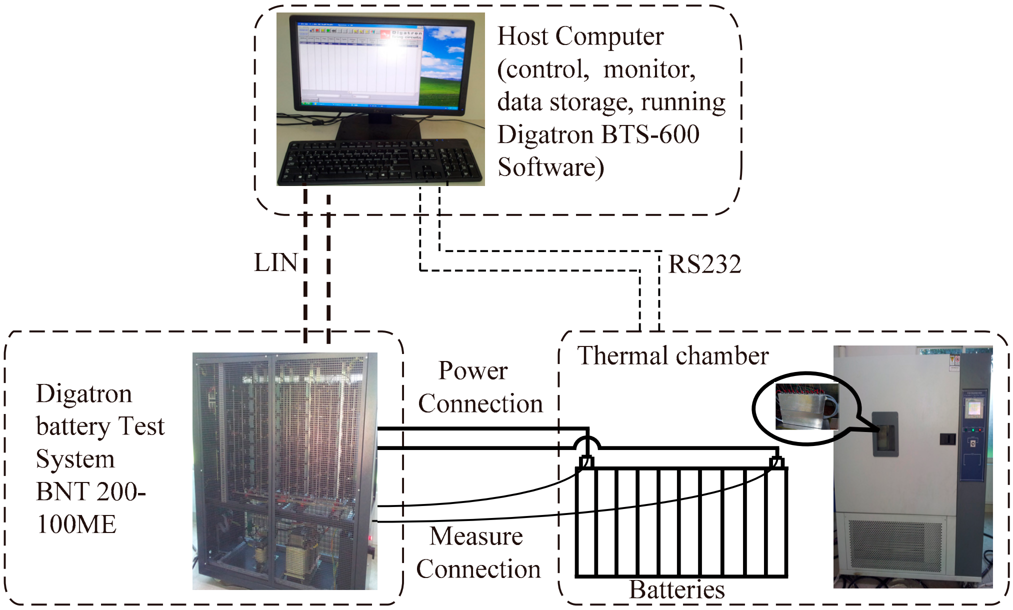

Figure 3. Battery pack testing device.

The cooling system of the battery package is shown in Figure 4. Considering that it is important to guarantee good insulation and contact between every single battery and the cooling plate, we bond the cooling plate and the batteries by coating conductive silicone, which can reduce the contact thermal resistance, as well as guarantee the insulation between each battery and the cooling plate. The inlet and outlet of the cooling liquid are, respectively, deployed on the sides of the cooling plate, and the pipes used for the flow of the cooling medium (the mixture of water and ethylene glycol) are built into the cooling plate. In so doing, it contributes to the cooling of each battery via the cooling plate. That is to say, when the batteries are in work, the heat is transferred from the batteries to the surfaces of the cooling plate, and then it is taken away by the cooling medium in the inner pipes, and finally, the heat is dissipated to the air via the air-cooled condenser.

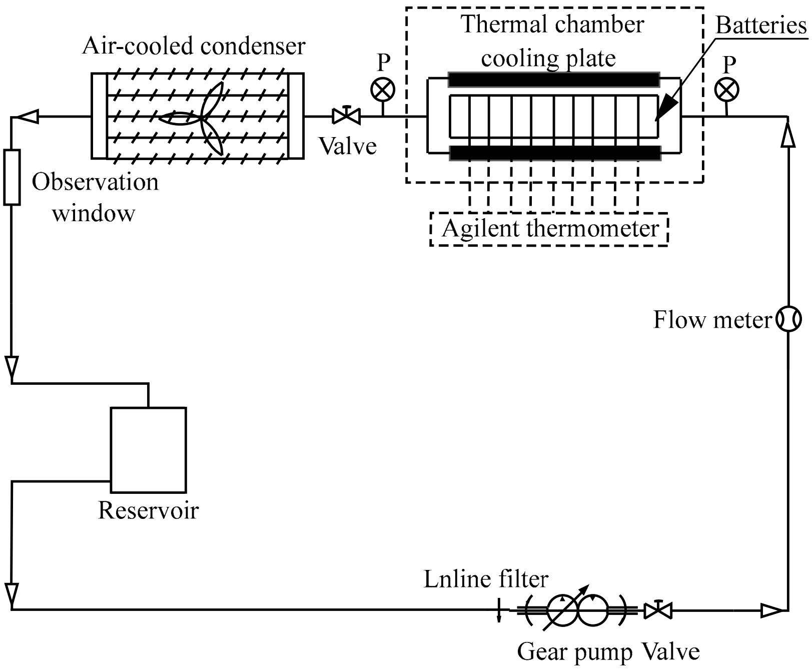

Figure 4. Battery pack testing device for cooling and heating.

The deployments of the temperature sensors with a total number of 20 on the surfaces of batteries are shown in Figure 5. For each battery, we deploy temperature sensors on the upper and lower half of the battery surface in Figure 6. An Agilent thermometer is used to measure the temperature rise of each temperature sensor when the batteries are at work. The device named Digatron BNT 200-100 ME is used to control the current. A gear pump is used to provide power for the cooling medium. A meter is used to measure the flow of the cooling medium.

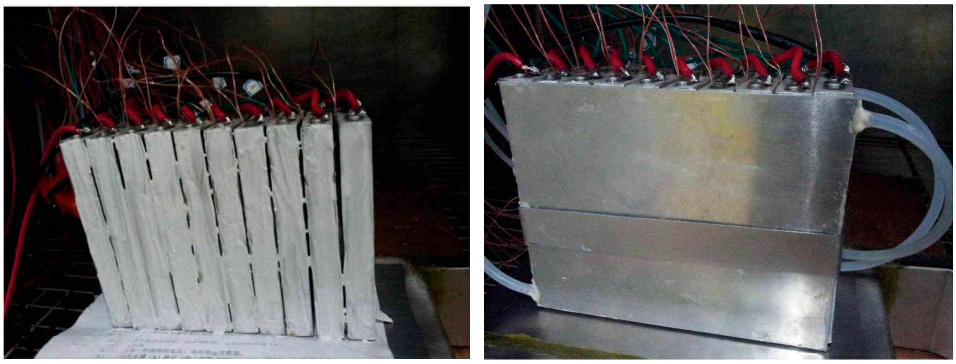

Figure 5. Battery pack module.

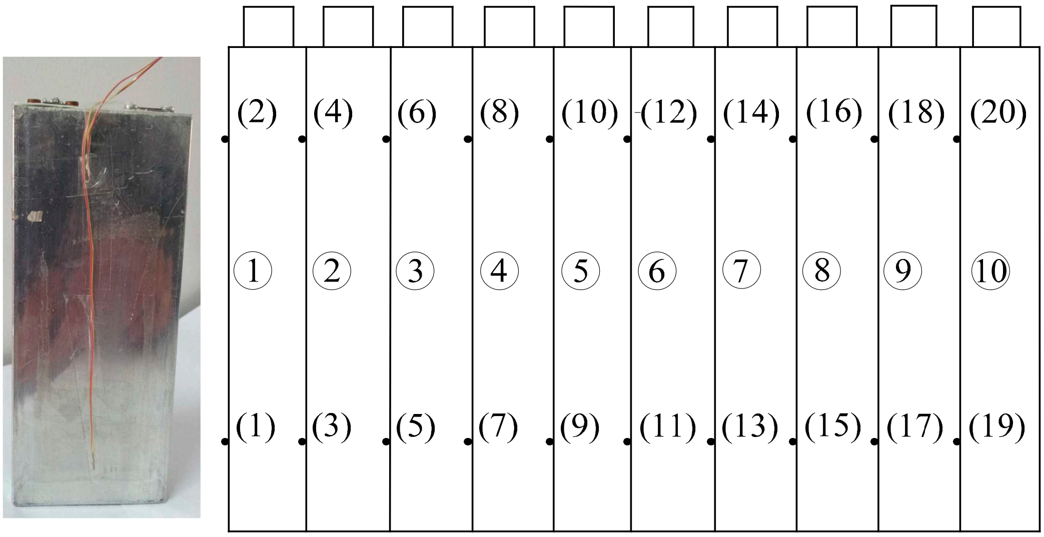

Figure 6. Comparison of the temperature difference and maximum temperature in the module.

2.3. Comparison of the Numerical and Experimental Results

In order to investigate the heat generation performance of a battery package during discharge, it is firstly charged at a constant current of 3 A (0.3 C) in a thermal chamber where the temperature is set to be 25 °C until the battery voltage reaches 36.5 V and 3.65 V; it is charged continuously at a constant voltage of 3.7 V (0.05 C) until the battery voltage reaches 37 V and 3.7 V, and then it is placed in the thermal chamber for 3 h. In the thermal chamber with a temperature of 25 °C, the batteries are discharged at a constant current of 20 A (2 C), and the cut-off voltage is 25 V and 2.5 V. The temperature of the inlet cooling medium is 23 C, and the flow rate is 0.1 L/min. After discharging, the maximum and minimum temperatures of each battery in the experiments and simulations are shown in Figure 7, and the temperature differences between experimental and simulation results can be seen in Figure 8.

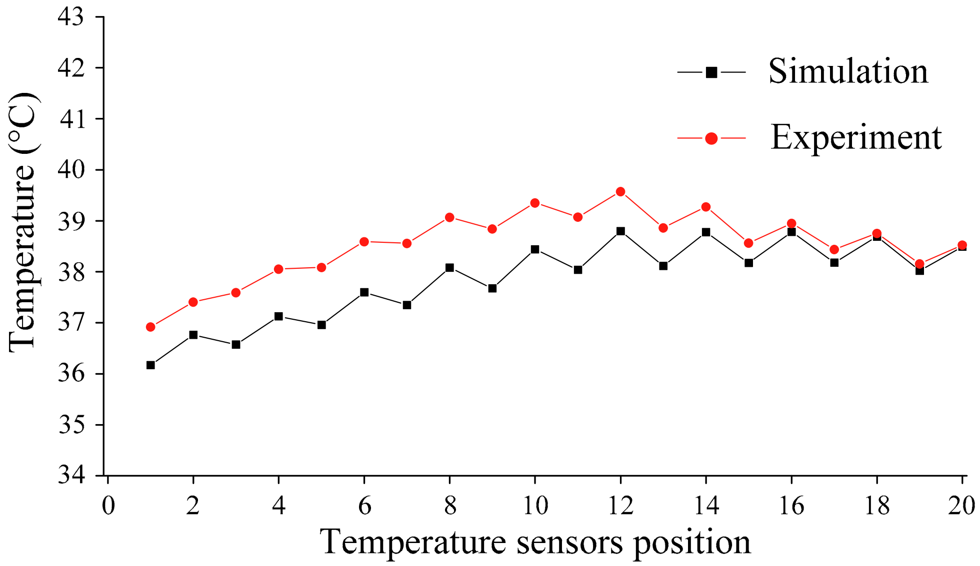

Figure 7. Comparison of the numerical and experimental results in terms of the temperature.

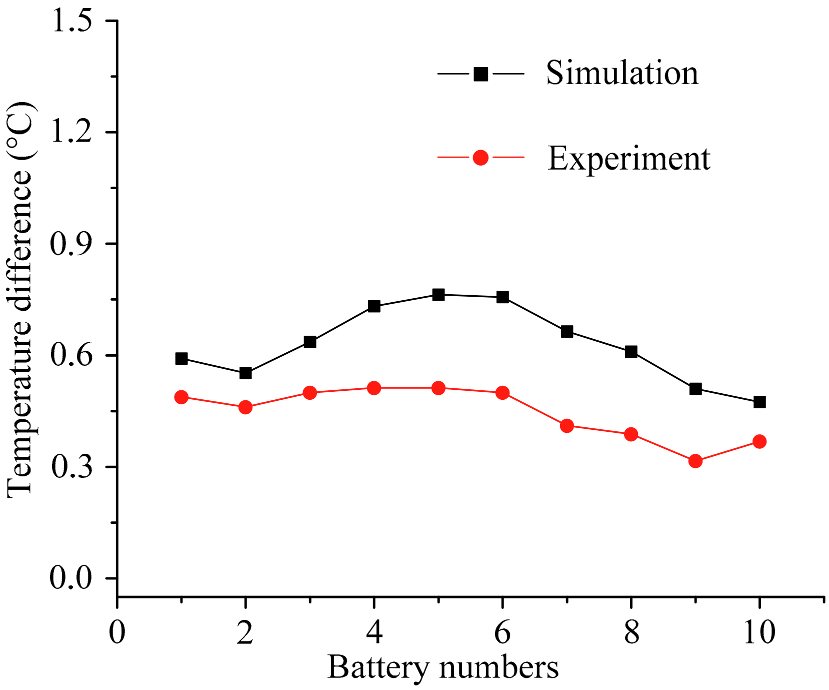

Figure 8. Experimental and simulation results of the temperature difference of a battery pack.

From Figure 7, we can see that the measured experimental maximum temperature appears in the fifth battery, because the batteries in the package are in contact with each other (see Figure 5), and the contact areas of the 1st and 10th batteries with air are the largest. Besides, the inlet of the cooling plate is in the first battery, thus resulting in relatively lower temperatures in the 1st to third batteries. In the numerical simulations, we mainly consider the internal resistance heating of the battery and neglect the chemical reaction heat; therefore, the maximum temperatures in the simulations are lower than the corresponding ones in the experiments; however, the general tendencies are the same.

Additionally, in Figure 7, when the horizontal axis is 7, the absolute error of the simulated and experimental temperature is the largest, with a value of 1.05 °C, and the experimental temperature is 38.55 °C. We can calculate that the maximal relative error of the simulated and experimental results is 2.7%. That is, the relative error is in the permissible scope. We can also find that as the measuring position changes, the simulated data has the same trend as the experimental data, and the simulation results are generally lower than the experimental results. Through the analysis, the reason is that: in the model, we set the battery package heat source as a constant body heat source, while the inner resistance of the battery is increased along with the time of discharge actually. It especially increases rapidly at the end of the discharge, which leads to an increase in Joule heat. Meanwhile, along with the discharge procedure, the inner side reaction of the battery also rises, which leads to a higher total amount of heat. Thus, the experiment results for every measuring point of the battery package are greater than those obtained from the simulation ones.

From Figure 8, the temperature difference obtained by numerical simulations in the first battery is smaller when compared with that in other batteries. That is because the heat source used in the numerical simulations is smaller than that in the experiments. Besides, the contact heat resistance between the cooling plate and batteries in the simulation model is not considered, i.e., the heat transfer in the middle part of the package in the simulations is faster than that in the experiments, which makes the simulated temperature differences in the middle part of the package larger than the corresponding experimental ones. In short, the experimental and simulated temperature differences are all small, i.e., they are less than 1 °C. The general tendencies of the experimental and simulated temperature differences for the 2nd to 10th batteries are the same.

3. Cooling Simulations of the Battery Package

In this work, we simulate the cooling performance of the battery package with a discharge rate of 2 C and compare the simulation results with the corresponding experimental outcomes to validate the effectiveness of the simulation method. Then, we calculate a group of cases where the discharge rates range from 1 C/cell to 4 C/cell, the liquid flow rate from 0.1 L/min to 20 L/min, and the inlet temperature from 5 °C to 40 °C.

3.1. Module

Figure 9 shows the geometric model of the liquid cooling heat dissipation system of the battery package. We can see that two cooling plates of equal dimensions are placed on two sides of the package, respectively. Pipes are built into each cooling plate for the purpose of taking away the heat, which is transferred from the batteries by means of the cooling medium. In this work, the ethylene glycol water solution is used as the cooling medium.

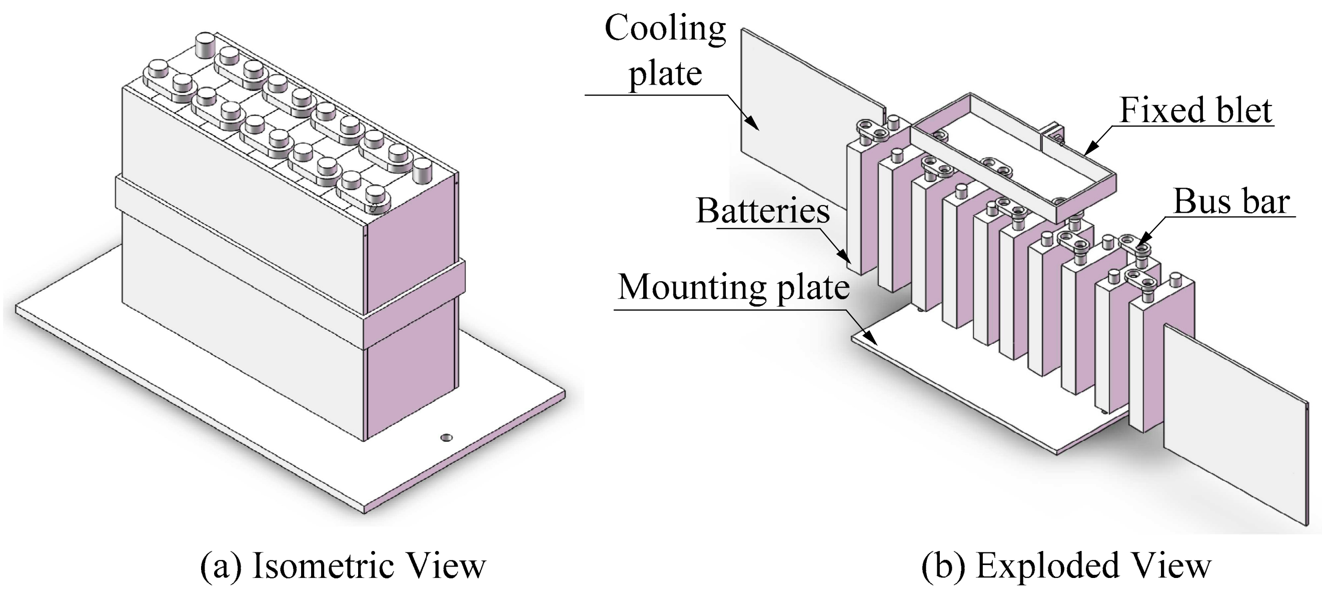

Figure 9. The geometry of the battery pack module.

In the simulations, the amount of the generated heat (see Equation (1)) applied to each battery is equal to that in the experiments. The input parameters are listed in Table 2. The heat conductivity coefficient of a battery is anisotropic, and we can evaluate the heat conductivity coefficient of a battery in three directions by using the principles of parallel and series resistance, as shown in Figure 1.

3.2. Mathematical Model

The simulations, including the fluid flow and heat transfer in the cooling plates, are conducted by means of FLUENT, where three-dimensional incompressible Navier–Stokes equations and a standard k-ε model are used. Besides, the so-called SIMPLE method is employed for iteration. In the SIMPLE algorithm, the solution is assumed to be terminated once the residuals of the x- and y- velocity equations are smaller than 10^{-7}. We have numerically confirmed that all the output parameters are converged by means of this termination condition. The governing equations are given as follows:

$$\frac{\partial u_j}{\partial x_j} \tag{3}$$

$$\rho\left(\frac{\partial u_i}{\partial t}+u_j\frac{\partial u_i}{\partial x_j}\right)=-\frac{\partial p}{\partial x_i}+\frac{\partial}{\partial x_j}\left(\mu\frac{\partial u_i}{\partial x_j}\right) \tag{4}$$

$$\rho c_p\left(\frac{\partial T}{\partial t}+u_j\frac{\partial T}{\partial x_j}\right)=\frac{\partial}{\partial x_j}\left(k\frac{\partial T}{\partial x_j}\right) \tag{5}$$

Only steady state condition is considered in this work, which takes the following forms:

$$\frac{\partial u_j}{\partial x_j} \tag{6}$$

$$\rho u_j\frac{\partial u_i}{\partial x_j}+\frac{\partial p}{\partial x_i}=\frac{\partial}{\partial x_j}\left(\mu\frac{\partial u_i}{\partial x_j}\right) \tag{7}$$

$$\rho c_p u_j\frac{\partial T}{\partial x_j}=\frac{\partial}{\partial x_j}\left(k\frac{\partial T}{\partial x_j}\right) \tag{8}$$

where u and x represent the velocity and direction vectors in Cartesian space; ρ is the density; p is the pressure; μ is the fluid viscosity; c_p is the specific heat capacity; T is the temperature; k is the thermal conductivity.

3.3. Boundary Condition

In order to model the working performance of the battery package accurately, we apply different heat sources during simulations so as to describe the different heat generated under different working conditions. During simulations, we cool the batteries by setting different flow rates and different inlet temperatures of the cooling liquid. The boundary conditions are listed in Table 3.

The battery surfaces that are in contact with the air are cooled via air-free convection. Apart from the surfaces that are in contact with the batteries, the other surfaces of the cooling plate are also cooled via air-free convection. Because the batteries are placed in the battery pack, the airflow is poor. We assume that the convective heat transfer coefficient is equal to 2 W/(m^2·K). Radiation heat transfer is neglected. Considering that isothermal compressibility and expansion coefficient are all small, we neglect the influence of liquid expansion on its density, viscosity, and heat conductivity coefficient. The cooling liquid is assumed to be incompressible. The physical parameters of the cooling plate do not vary over time, and thus the liquid cooling plate works under and thus steady conditions. The inlet boundary conditions are that the mass flow rate is steady, and the temperature is

300 K. With respect to the outlet boundary condition, we set it to be a pressure outlet with a value of 0 Pa. Because there are several elbow pipes in the cooling plate, we adopt a turbulence model in the calculation.

Table 3. Description of the input parameter and quantities of interest.

Boundary Conditions	Definition	Range
Cell heat loss Q	It denotes the heat loss of a given cell under various working conditions.	1–4 C/Cell
Coolant inlet	It reflects the temperature of the coolant at the inlet of the	5–40 °C
Temperature T_{in}	cooling plate in the cases of cooling and preheating.	40–70 °C
Coolant volume-ric flow rate V	It denotes the volumetric flow rate of the coolant, which is converted to a mass flow rate in FLUENT.	0.1–20 L/min
T_{max}	It means the highest temperature in the package.	Output
ΔT	It reflects the difference between the maximum and minimum cell temperatures in the module. $T_{max} - T_{min}$	Output

3.4. Numerical Analyses

The same boundary conditions in the experiments are applied in the numerical simulations. The inlet temperature of the liquid cooling medium is 23 °C, and the flow rate is 0.1 L/min. The maximum and minimum temperatures of each battery after discharging are shown in Figure 7. From this figure, we can see that the tendencies of the simulation results are basically inconsistent with those of the corresponding experiment outcomes. The temperature difference of each battery can be seen in Figure 8. From this figure, we can see that the simulated temperature difference of each battery agrees with the corresponding experiment result apart from that of the first battery. After validating the effectiveness of the simulation method, we investigate the cooling performance of the battery package with a discharge rate of 1 °C to 4 °C, where the flow rate is 0.5 L/min, and the inlet temperature ranges from 5 °C to 40 °C. The maximum temperature and temperature difference of the battery package versus fluid inlet temperature curves is plotted in Figures 10 and 11. Then, we investigate the cooling performance of the battery package with a discharging rate of 1 °C to 4 °C, where the inlet temperature is set to 25 °C and the flow rate ranges from 0.1 L/min to 20 L/min. The maximum temperature and temperature difference of the battery package versus volumetric flow rate curves are plotted in Figures 12 and 13. Finally, we investigate the cooling performance of the battery package with the discharging rate ranging from 1 °C to 4 °C, flow rate from 0.1 L/min to 20 L/min, and inlet temperature from 5 °C to 40 °C. The maximum temperature and temperature difference of the battery package versus flow rate and inlet temperature curves are plotted in Figures 14 and 15.

Figure 10 shows that the maximum temperature of the battery package rises with the increase of the discharge current. The maximum temperature difference of the battery package is 15 °C when the discharge rates are between 4 °C and 3 °C; it is 10 °C when the discharge rates are between 3 °C and 2 °C; and it is 7 °C when the discharge rates are between 2 °C and 1 °C. Besides, the maximum temperature of the battery package rises with the increase of the inlet fluid temperature when the discharge rates are kept constant. For example, when the discharge rate is 1 °C, the maximum temperature is 7.5 °C with an inlet fluid temperature of 5 °C; however, it is 41.3 °C with an inlet fluid temperature of 40 °C.

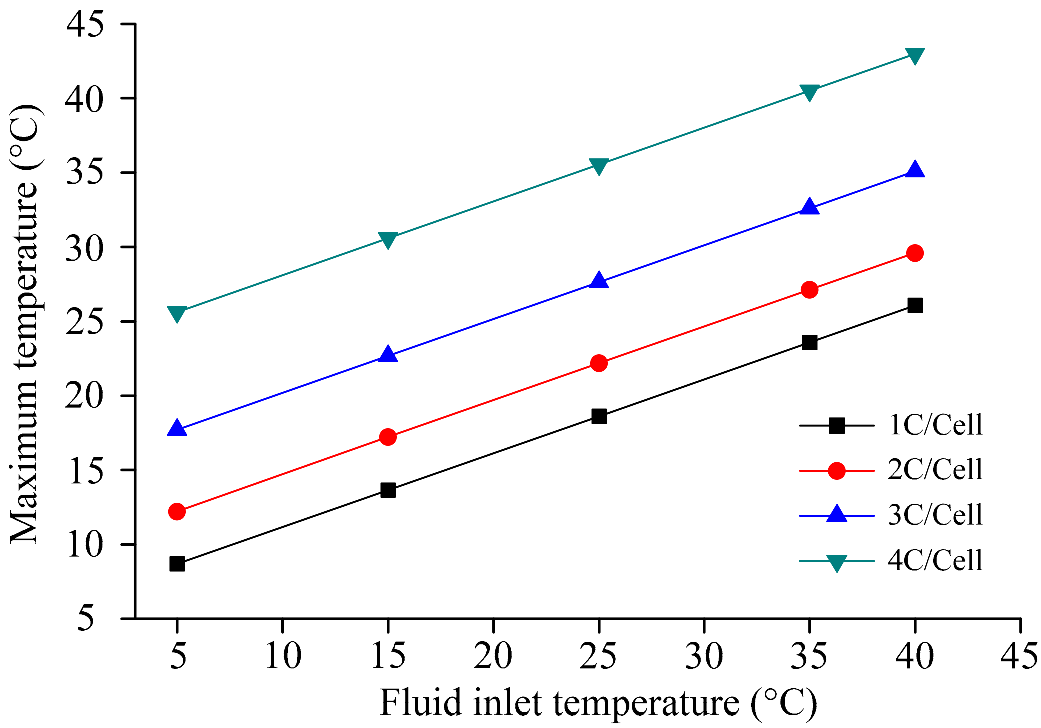

Figure 10. The battery surface maximum temperature versus fluid inlet temperature curves with discharging rates ranging from 1 C to 4 C.

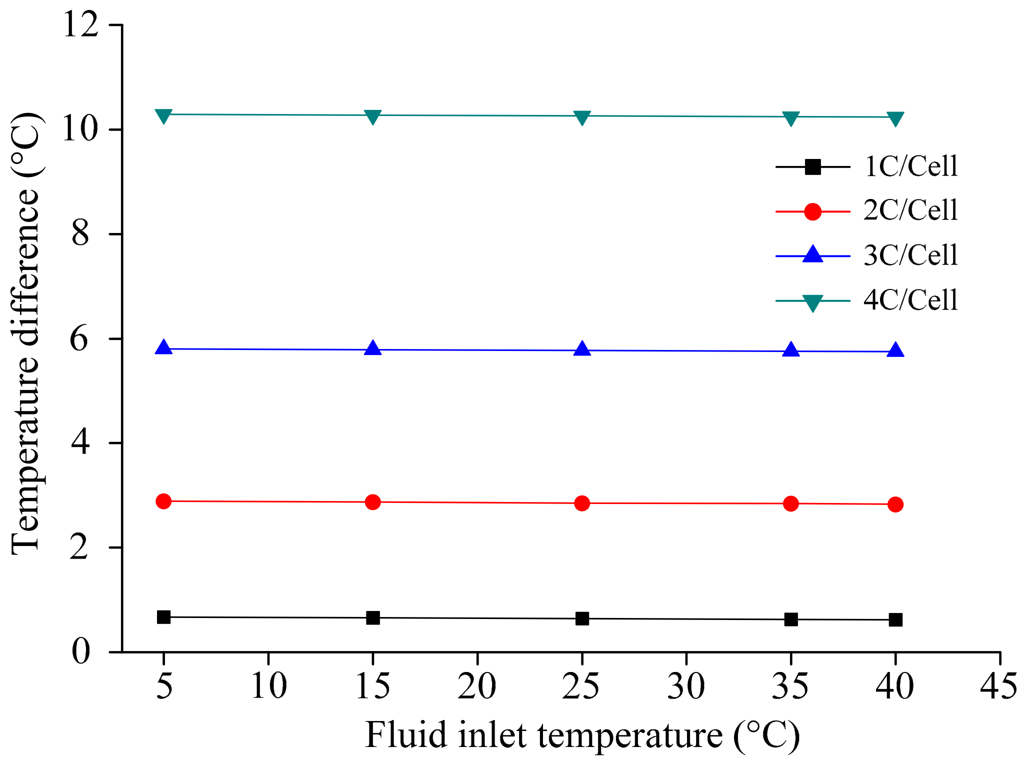

Figure 11. The battery surface temperature difference versus fluid inlet temperature curves with discharge rates ranging from 1 C to 4 C.

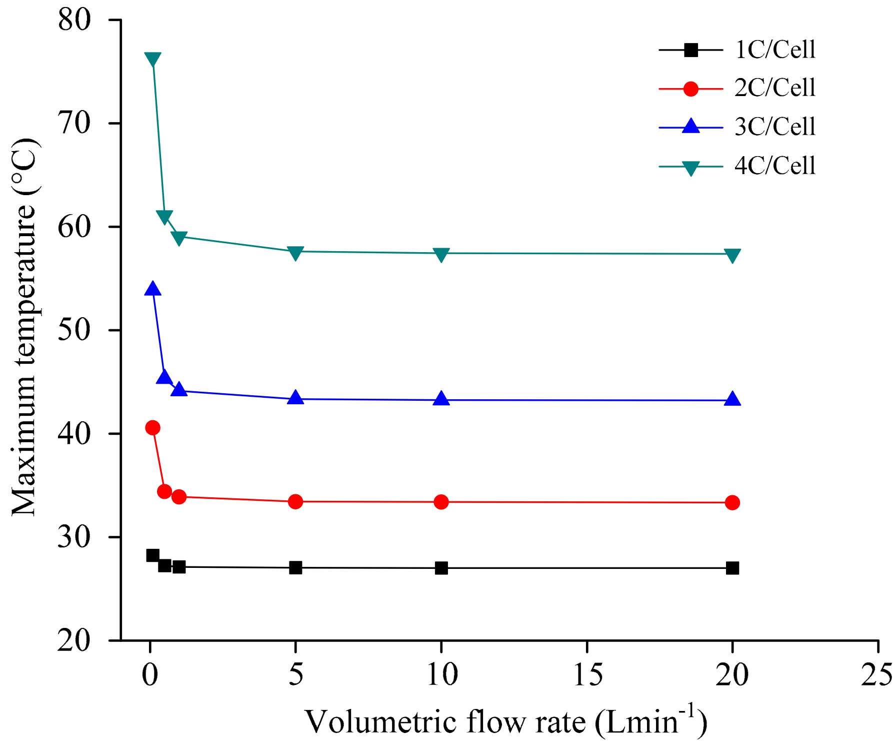

Figure 12. The battery surface temperature difference versus fluid inlet temperature curves with discharging rates ranging from 1 C to 4 C.

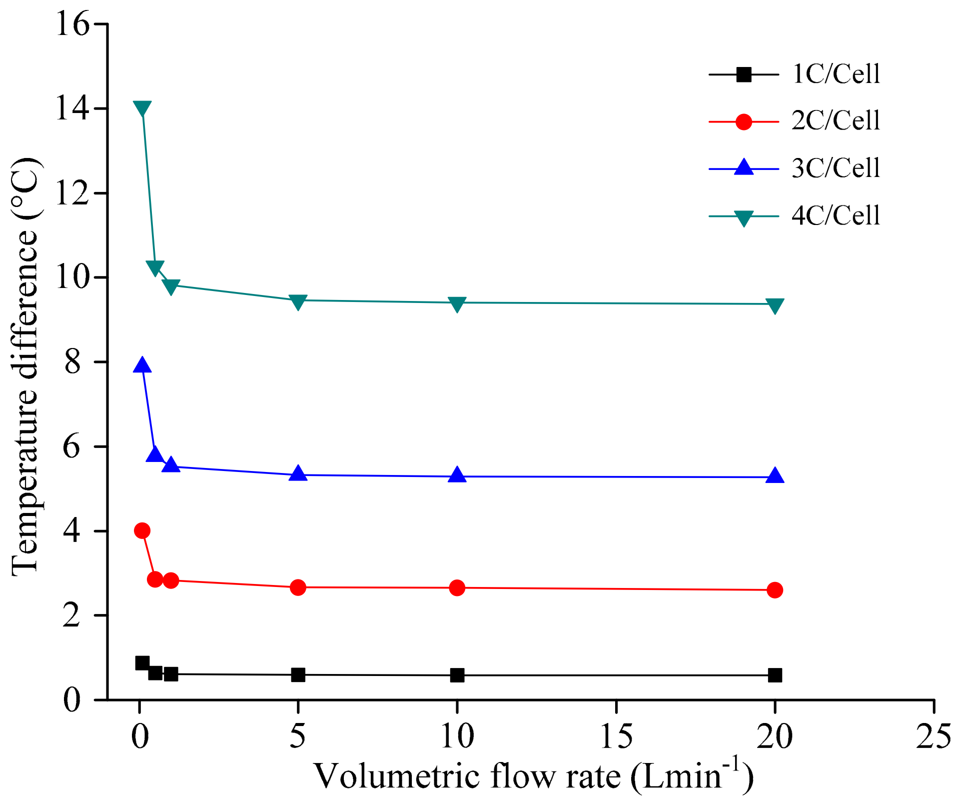

Figure 13. The battery surface temperature difference versus volumetric flow rate curves with discharge rates ranging from 1 C to 4 C.

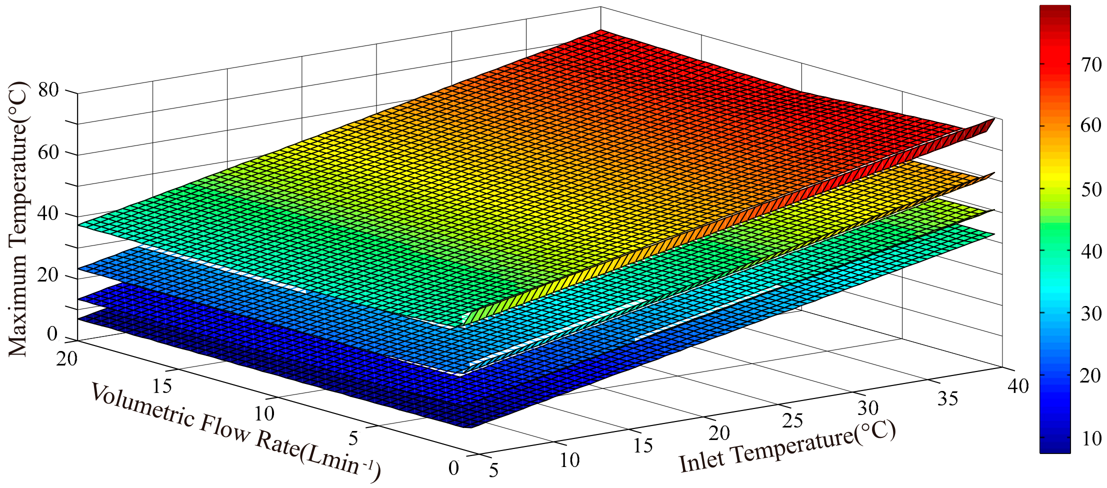

Figure 14. The maximum temperatures of the battery package with discharge rates ranging from 1 C to 4 C.

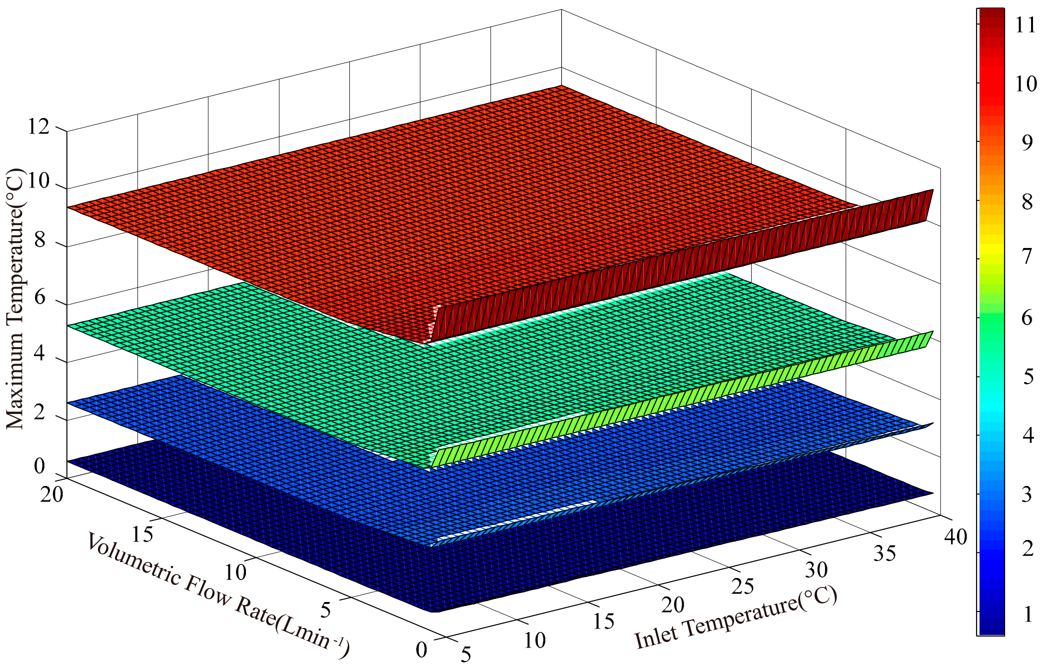

Figure 15. The temperature differences of the battery package with discharge rates ranging from 1 C to 4 C.

Figure 11 shows that the temperature differences of the battery package are almost the same, along with the changes in the inlet fluid temperatures when the discharge rates are kept constant. The temperature difference rises with the increase of the discharge current. The temperature difference of the battery package is 10 °C with a discharge rate of 4 °C; it is 5.7 °C with a discharge rate of 3 °C; it is 2.8 °C with a discharge rate of 2 °C; it is 0.6 °C with a discharge rate of 1 °C. However, the temperature differences are almost not changed when the package is discharged at the same rates. In other words, the inlet fluid temperature has little influence on the temperature uniformity of the battery package. Figure 12 shows that the maximum temperature of the battery package remains unchanged when the liquid flow is larger than 0.5 L/min under the same discharge condition. It only rises along with the increase of the discharge current. That is to say, when the liquid flow is larger than a certain value, the liquid flow has little influence on the maximum temperature of the battery package. When the liquid flow is larger than 0.5 L/min, the maximum temperature of the package with a discharge rate of 4 °C is 15 °C larger than that with a discharge rate of 3 °C; the maximum temperature of the package with a discharge rate of 3 °C is 10 °C larger than that with the discharge rate of 2 °C; the maximum temperature of the package with the discharge rate of 2 °C is 7 °C larger than that with the discharge rate of 1 °C. The maximum temperature increases dramatically when the flow is less than 0.5 L/min.

Figure 13 shows that the temperature difference of the battery package remains to be unchanged when the liquid flow is larger than 0.5 L/min under the same discharge conditions. It only rises along with the increase of the discharge current. That is to say, when the liquid flow is larger than a certain value, the liquid flow has little influence on the temperature difference of the battery package. The temperature difference of the package with a discharge rate of 4 °C is 10 °C; it is 5.7 °C with a discharge rate of 3 °C; it is 2.8 °C with a discharge rate of 2 °C; and it is 0.6 °C with a discharging rate of 1 °C. The temperature difference increases dramatically when the flow is less than 0.5 L/min.

Figure 14 shows the cooling performance of the battery package, where the discharge rates range from 1 °C to 4 °C, the liquid flow rates from 0.1 L/min to 20 L/min, and the inlet temperatures from 5 °C to 40 °C. From this figure, we can clearly see the influences of the liquid flow and the inlet temperature on the maximum temperatures of the batteries. When the batteries generate a lot of heat, the cooling performance is more obvious by changing the liquid flow and the inlet temperature. The maximum temperature of the package is lower than 50 °C when the working conditions are: discharging rates are 1 °C and 2 °C; flow rates range from 0.1 L/min to 20 L/min; inlet temperatures are from 5 to 40 °C. When the battery package is working with discharging rates of 3 °C and 4 °C, in order to keep the package working in an optimum temperature range, one can lower the inlet temperature and enlarge the flow rate. In the case of discharging with a rate of 3 °C, we can control the maximum temperature of the package within 50 °C by setting the inlet temperature lower than 35 °C and the flow rate larger than 5 L/min. Additionally, in case of discharging with a rate of 4 °C, we can control the maximum temperature of the package within 50 °C by setting the inlet temperature lower than 15 °C and the flow rate larger than 0.5 L/min.

The temperature difference is another important index for the evaluation of the cooling performance of a battery package. Figure 15 shows the temperature differences of the package with different heating power. When the package is discharged with a rate lower than 3 °C and the flow rate is larger than 0.5 L/min, the temperature difference of each battery is lower than 5.7 °C. However, if the package is discharged at a rate of 4 °C, no matter how to adjust the flow rates and the inlet temperatures, the temperature differences exceed 10 °C, which is beyond the scope of permission. For the four working conditions above, we can see that the temperature differences of batteries are almost the same, which means that the inlet temperature has little influence on temperature uniformity.

4. Simulations and Experiments of Battery Heating

EVs should be able to work at a wide temperature range. In recent decades, the cooling performance of batteries has received universal attention from researchers. However, little literature has reported the influence of low temperatures on the performance of batteries. Normally, the power batteries start to work when the temperature reaches above 0 °C, and their lower limit range of the optimum working temperature is 10 °C. This paper heats the battery package by controlling the liquid flow rate and the inlet temperature so as to make it reach a good used condition with less time and power consumption, which will provide a reference for the BTMS.

4.1. Experimental Validation

The experiment scheme of battery heating is the same as that of battery cooling. In this experiment, the heating source of the liquid is an electric heater, and the warmed liquid can heat every single battery via pipes in the cooling plate. After heating to 50 °C, the liquid is kept warm, and the flow rate is 0.1 L/min. Because the temperature of the package is not in its optimum working temperature range during the preheating process, batteries are not working during experiments, i.e., the thermal load is always zero. The initial temperature of each battery is 0 °C. The relationships between the heating time and the rising temperature of the ten batteries are shown in Figure 16.

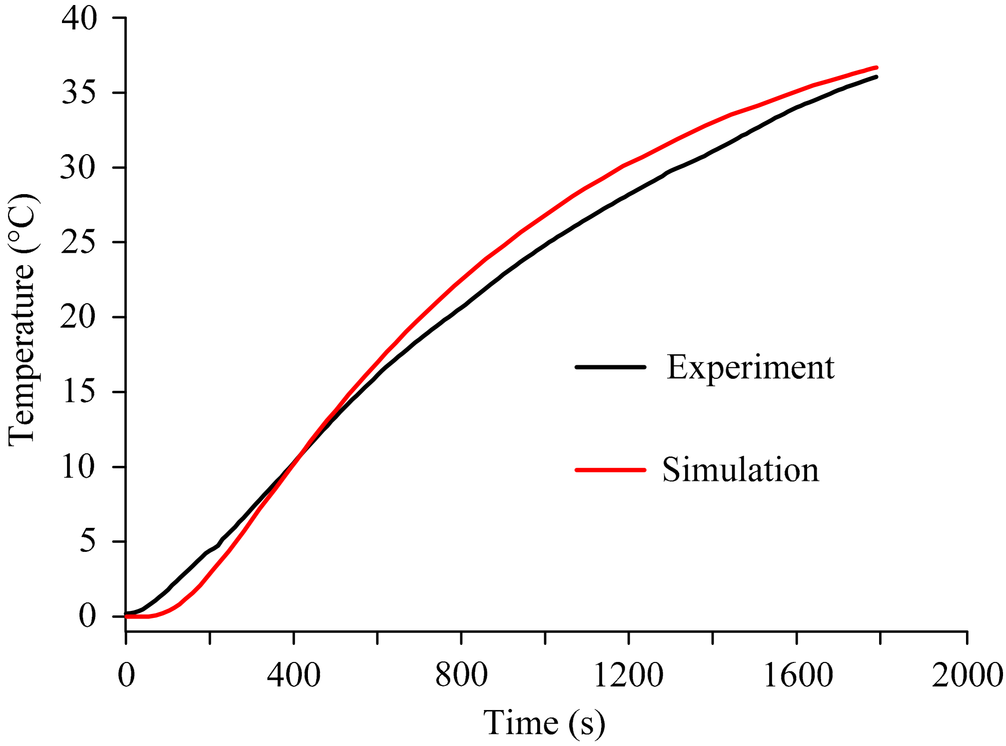

Figure 16. Comparisons of the battery surface temperature obtained from the simulation and experiment ranged from 1 C to 4 C.

From this figure, we can see that the simulation result agrees well with the corresponding experimental one. The final temperature in the experiment is 36.67 °C; however, the simulated final temperature is 36.59 °C. The battery temperature increases with the rise of the heating time. In the initial stage of the preheating process, the average experimental temperature is lower than the simulated one; they are equal at about 400 s; after that, the experimental temperature is higher than the simulated one. That is because we neglect the contact thermal resistance in the simulations, which is caused by the gaps between a part of the batteries and the cooling plate.

4.2. Numerical Analyses

The numerical models, including the liquid and the cooling plate for the preheating simulations, are the same as those for the cooling simulations. The boundary conditions are the inlet temperature of the liquid is 50 °C; the flow rate is 0.1 L/min; ambient temperature is 0 °C; pressure output with a value of 0 Pa is set; surfaces are set to be adiabatic, apart from the contact surfaces between batteries and between batteries and the cooling plate. Though the cooling plate is to be working in the battery package for a long time, its physical parameters will not change over time, i.e., the cooling plate is working under a steady state. However, considering that we need to obtain the steady field at a certain time during preheating, we employ transient analysis during simulations. The simulation results can be found in Figure 16. After validation of the simulation method, we perform another two numerical cases, where the ambient temperatures are −5 °C and −15 °C, respectively. The simulation results are shown in Figure 17.

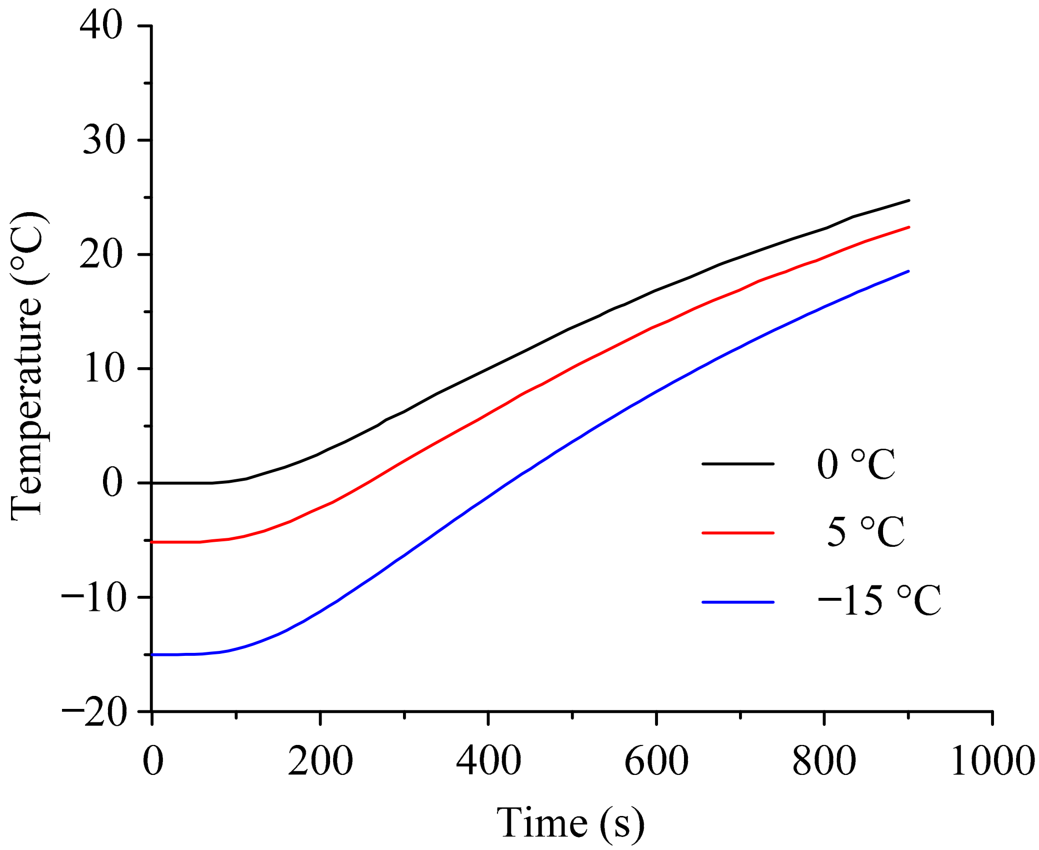

Figure 17. The battery temperature versus time curves with three ambient temperatures of 0 °C, −5 °C, and −15 °C.

Numerical simulation results show that the preheating process slows down with the decrease in the initial battery temperature. For the battery with an initial temperature of 0 °C, it takes 210 s to heat the battery up to 5 °C; however, it takes 340 s and 500 s for the initial battery temperatures of −5 °C and −15 °C, respectively.

Because the heating process is relatively slow when the flow rate is 0.1 L/min, we also numerically investigate the influence of the flow rate on the heating performance. In the simulations, the ambient temperature is −15 °C; the batteries are not in work; the inlet temperature of the liquid is 50 °C; the flow rates are 0.1 L/min, 0.5 L/min, and 5 L/min, respectively. The simulation results can be found in Figure 18.

From Figure 18, we can see that the preheating process speeds up with the increase in the flow rate. When the flow rate is 0.1 L/min, it takes 550 s to heat the battery from −15 °C to 5 °C. However, when the flow rate is 0.5 L/min, it only needs 300 s, whose heating time is 45.5% shorter than that in the preheating process with a flow rate of 0.1 L/min. When the flow rate is 5 L/min, it only needs 260 s, whose heating time is 52.7% shorter than that in the preheating process, with a flow rate of 0.1 L/min. Consequently, one can use a large flow rate to speed up the healing process so as to save time.

In order to investigate the inlet temperature on the heating performance, we perform three numerical cases, where the inlet temperatures are 10 °C, 30 °C, and 50 °C, respectively. The other conditions are the same as those in the heating simulations above. The simulation results can be found in Figure 19.

In Figure 19, we can see that the preheating process speeds up with the increase in the inlet temperature. When the inlet temperature is 10 °C, it takes 16 min to heat the battery to a temperature of 5 °C. However, when the inlet temperature is 30 °C, it only needs 6.5 min, whose heating time is 59.4% shorter than that in the preheating process with an inlet temperature of 10 °C. When the inlet temperature is 50 °C, it only needs 5 min, whose heating time is 68.7% shorter than that in the preheating process with an inlet temperature of 10 °C. Consequently, one can use a high inlet temperature to speed up the heating process so as to save time.

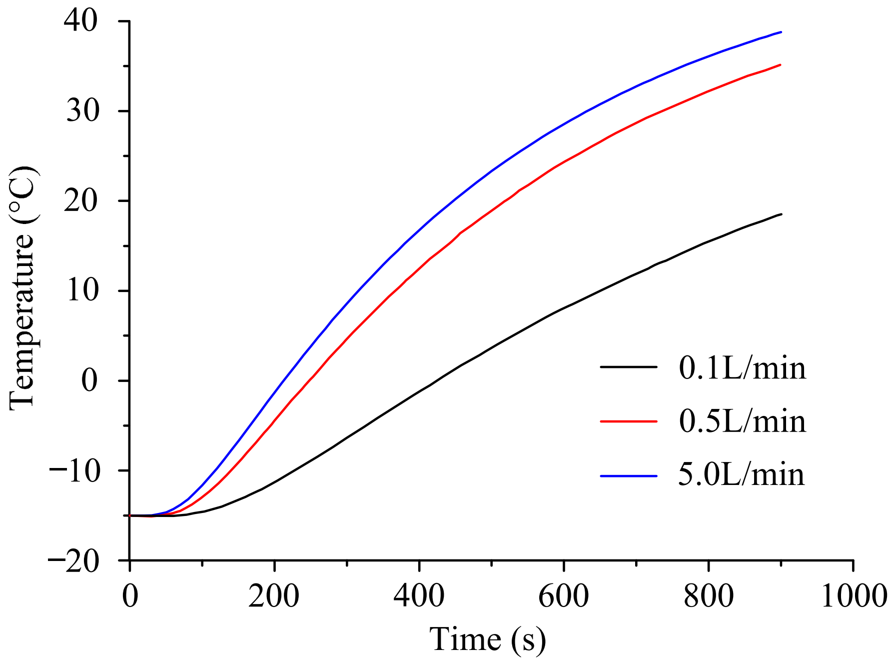

Figure 18. The battery temperature versus time curves with three flow rates of 0.1 L/min, 0.5 L/min, and 5 L/min.

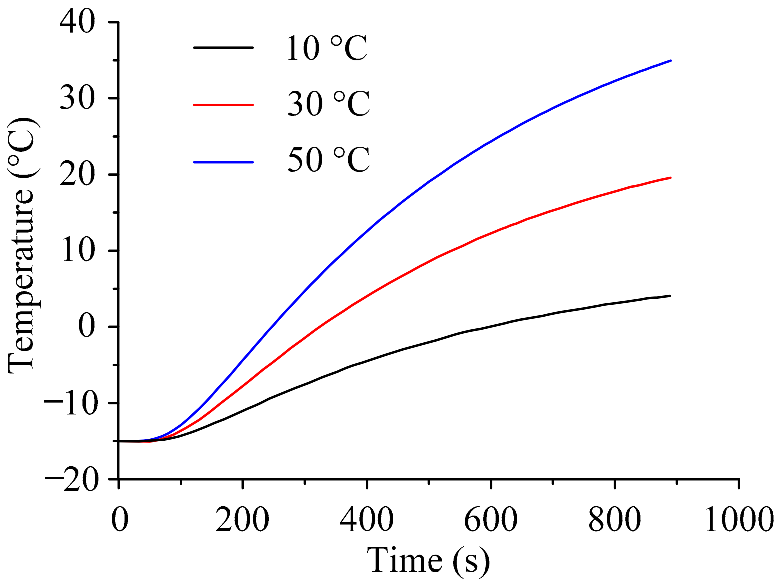

Figure 19. The battery surface temperature versus time curves with three inlet temperatures of 10 °C, 30 °C, and 50 °C.

As a result, one may need to install heating and thermal insulation systems for the battery package in EVs in cold regions, which will make the preheating process unnecessary after a short time of parking, or provide a relatively high initial temperature after a long-time parking. Besides, it also contributes to the energy recovery, which can be used to warm the passenger compartment or provide a heating source for the heat pump, thereby extending the driving mileage of EVs.

5. Conclusions

In this paper, we design a liquid cooling and heating device for the battery packaging. Ten lithium-ion batteries are connected in series to be a package. Liquid cooling experiments with a discharge rate of 2 C and preheating experiments with a temperature of 0 °C are carried out for the battery package. A thermoelectric couple is used to gather the temperature information of the package so as to perform cooling and heating analyses. A three-dimensional numerical model for the battery package is built, whose effectiveness is validated by comparing the simulation results with the corresponding experimental outcomes in terms of battery surface temperature and temperature difference. In the cooling simulations, we investigate the influences of the liquid flow rate and the inlet temperature on the maximum temperature and temperature difference of batteries. When the batteries generate a lot of heat, the cooling effects are obvious by changing the flow rate and the inlet temperature. When the inlet temperature is set to be constant, and the flow rate is less than 0.5 L/min, the flow rate has a significant influence on the maximum temperature and the temperature difference of the package; however, when the flow rate is larger than 0.5 L/min, it has little effect on the maximum temperature and the temperature difference. The inlet temperature has little influence on temperature uniformity. In the preheating simulations, we investigate the influences of the flow rate and the inlet temperature on the preheating performance. Numerical results show that large flow rates and high inlet temperatures are able to speed up the preheating process, thereby saving time for the drivers.

Author Contributions: Conceptualization, J.X.; methodology, J.X. and D.W.; validation, D.W. and J.X.; formal analysis, D.W.; investigation, D.W. and J.X.; data curation, J.X.; writing—original draft preparation, D.W.; writing—review and editing, D.W. and J.X.; supervision, D.W.; project administration, D.W. and J.X.; funding acquisition, D.W. All authors have read and agreed to the published version of the manuscript.

Funding: This work is supported by the Natural Science Foundation of Xinjiang Uygur Autonomous Region (No. 2021D01C115).

Data Availability Statement: https://www.mdpi.com/1996-1944/15/19/6880, https://www.mdpi.com/1996-1944/16/4/1708, https://www.mdpi.com/2075-1702/11/6/657/htm.

Conflicts of Interest: The authors declare no conflict of interest.

References

1. Zeng, Y.; Chalise, D.; Lubner, S.D.; Kaur, S.; Prasher, R.S. A review of thermal physics and management inside lithium-ion batteries for high energy density and fast charging. *Energy Storage Mater.* **2021**, *41*, 264–288. [CrossRef]
2. Gao, Z.; Xie, H.; Yang, X.; Niu, W.; Li, S.; Chen, S. The Dilemma of C-Rate and Cycle Life for Lithium-Ion Batteries under Low Temperature Fast Charging. *Batteries* **2022**, *8*, 234. [CrossRef]
3. Zappen, H.; Fuchs, G.; Gitis, A.; Sauer, D.U. In-operando impedance spectroscopy and ultrasonic measurements during high-temperature abuse experiments on lithium-ion batteries. *Batteries* **2020**, *6*, 25. [CrossRef]
4. Lander, L.; Kallitsis, E.; Hales, A.; Edge, J.S.; Korre, A.; Offer, G. Cost and carbon footprint reduction of electric vehicle lithium-ion batteries through efficient thermal management. *Appl. Energy* **2021**, *289*, 116737. [CrossRef]
5. Alihosseini, A.; Shafaee, M. Experimental study and numerical simulation of a Lithium-ion battery thermal management system using a heat pipe. *J. Energy Storage* **2021**, *39*, 102616. [CrossRef]
6. Thakur, A.K.; Prabakaran, R.; Elkadeem, M.R.; Sharshir, S.W.; Arıcı, M.; Wang, C.; Zhao, W.; Hwang, J.-Y.; Saidur, R. A state of art review and future viewpoint on advance cooling techniques for Lithium–ion battery system of electric vehicles. *J. Energy Storage* **2020**, *32*, 101771. [CrossRef]
7. Chiu, K.C.; Lin, C.H.; Yeh, S.F.; Lin, Y.H.; Huang, C.S.; Chen, K.C. Cycle life analysis of series connected lithium-ion batteries with temperature difference. *J. Power Sources* **2014**, *263*, 75–84. [CrossRef]
8. Wang, K.; Ouyang, D.; Qian, X.; Yuan, S.; Chang, C.; Zhang, J.; Liu, Y. Early Warning Method and Fire Extinguishing Technology of Lithium-Ion Battery Thermal Runaway: A Review. *Energies* **2023**, *16*, 2960. [CrossRef]
9. Zang, M.; Xie, J.; Ouyang, J.; Wang, S.; Wu, X. Investigation of temperature performance of Lithium-ion batteries for electric. In Proceedings of the 2014 IEEE Conference and Expo Transportation Electrification Asia-Pacific (ITEC Asia-Pacific), Beijing, China, 31 August–3 September 2014; pp. 1–8.

10. Fayaz, H.; Afzal, A.; Samee, A.M.; Soudagar, M.E.M.; Akram, N.; Mujtaba, M.A.; Islam, T.; Ağbulut, Ü.; Saleel, C.A. Optimization of thermal and structural design in lithium-ion batteries to obtain energy efficient battery thermal management system (BTMS): A critical review. *Arch. Comput. Methods Eng.* **2022**, *29*, 129–194. [CrossRef]
11. Weng, J.; Huang, Q.; Li, X.; Zhang, G.; Ouyang, D.; Chen, M.; Yuen, A.C.Y.; Li, A.; Lee, E.W.M.; Yang, W.; et al. Safety issue on PCM-based battery thermal management: Material thermal stability and system hazard mitigation. *Energy Storage Mater.* **2022**, *53*, 580–612. [CrossRef]
12. Yuan, Q.; Zhao, F.; Wang, W.; Zhao, Y.; Liang, Z.; Yan, D. Overcharge failure investigation of lithium-ion batteries. *Electrochim. Acta* **2015**, *178*, 682–688. [CrossRef]
13. Troxler, Y.; Wu, B.; Marinescu, M.; Yufit, V.; Patel, Y.; Marquis, A.J.; Brandon, N.P.; Offer, G.J. The effect of thermal gradients on the performance of lithium-ion batteries. *J. Power Sources* **2014**, *247*, 1018–1025. [CrossRef]
14. Lin, J.; Liu, X.; Li, S.; Zhang, C.; Yang, S. A review on recent progress, challenges and perspective of battery thermal management system. *Int. J. Heat Mass Transf.* **2021**, *167*, 120834. [CrossRef]
15. Zhang, Z.; Wei, K. Experimental and numerical study of a passive thermal management system using flat heat pipes for lithium-ion batteries. *Appl. Therm. Eng.* **2020**, *166*, 114660. [CrossRef]
16. Landini, S.; Leworthy, J.; O'Donovan, T.S. A review of phase change materials for the thermal management and isothermalisation of lithium-ion cells. *J. Energy Storage* **2019**, *25*, 100887. [CrossRef]
17. Mali, V.; Saxena, R.; Kumar, K.; Kalam, A.; Tripathi, B. Review on battery thermal management systems for energy-efficient electric vehicles. *Renew. Sustain. Energy Rev.* **2021**, *151*, 111611. [CrossRef]
18. Alnaqi, A.A. Numerical analysis of pressure drop and heat transfer of a Non-Newtonian nanofluids in a Li-ion battery thermal management system (BTMS) using bionic geometries. *J. Energy Storage* **2022**, *45*, 103670. [CrossRef]
19. Alaoui, C. Passive/active BTMS for EV lithium-ion batteries. *IEEE Trans. Veh. Technol.* **2018**, *67*, 3709–3719. [CrossRef]
20. Wang, M.; Teng, S.; Xi, H.; Li, Y. Cooling performance optimization of air-cooled battery thermal management system. *Appl. Therm. Eng.* **2021**, *195*, 117242. [CrossRef]
21. Wang, T.; Tseng, K.J.; Zhao, J.; Wei, Z. Thermal investigation of lithium-ion battery module with different cell arrangement structures and forced air-cooling strategies. *Appl. Energy* **2014**, *134*, 229–238. [CrossRef]
22. Zhang, J.; Shao, D.; Jiang, L.; Zhang, G.; Wu, H.; Day, R.; Jiang, W. Advanced thermal management system driven by phase change materials for power lithium-ion batteries: A review. *Renew. Sustain. Energy Rev.* **2022**, *159*, 112207. [CrossRef]
23. Khateeb, S.A.; Farid, M.M.; Selman, J.R.; Al-Hallaj, S. Design and simulation of a lithium-ion battery with a phase change material thermal management system for an electric scooter. *J. Power Sources* **2004**, *128*, 292–307. [CrossRef]
24. Mills, A.; Al-Hallaj, S. Simulation of passive thermal management system for lithium-ion battery packs. *J. Power Sources* **2005**, *141*, 307–315. [CrossRef]
25. Tran, T.H.; Harmand, S.; Sahut, B. Experimental investigation on heat pipe cooling for hybrid electric vehicle and electric vehicle lithium-ion battery. *J. Power Sources* **2014**, *265*, 262–272. [CrossRef]
26. Rao, Z.; Wang, S.; Wu, M.; Lin, Z.; Li, F. Experimental investigation on thermal management of electric vehicle battery with heat pipe. *Energy Convers. Manag.* **2013**, *65*, 92–97. [CrossRef]
27. Wang, Q.; Jiang, B.; Xue, Q.F.; Sun, H.L.; Li, B.; Zou, H.M.; Yan, Y.Y. Experimental investigation on EV battery cooling and heating by heat pipes. *Appl. Therm. Eng.* **2015**, *88*, 54–60. [CrossRef]
28. Ding, Y.; Ji, H.; Wei, M.; Liu, R. Effect of liquid cooling system structure on lithium-ion battery pack temperature fields. *Int. J. Heat Mass Transf.* **2022**, *183M*, 122178. [CrossRef]
29. Liu, R.; Chen, J.; Xun, J.; Jiao, K.; Du, Q. Numerical investigation of thermal behaviors in lithium-ion battery stack discharge. *Appl. Energy* **2014**, *132*, 288–297. [CrossRef]
30. Pesaran, A.; Kim, G.H. *Battery Thermal Management System Design Modeling*; National Renewable Energy Lab. (NREL): Golden, CO, USA, 2006.
31. Jarrett, A.; Kim, I.Y. Design optimization of electric vehicle battery cooling plates for thermal perfor-mance. *J. Power Sources* **2011**, *196*, 10359–10368. [CrossRef]
32. Xie, J.; Zang, M.; Wang, S.; Ge, Z. timization investigation on the liquid cooling heat dissipation structure for the lithium-ion battery package in electric vehicles. *Proc. Inst. Mech. Eng. Part D J. Automob. Eng.* **2017**, *231*, 1735–1750. [CrossRef]
33. Falcone, M.; Palka Bayard De Volo, E.; Hellany, A.; Rossi, C.; Pulvirenti, B. Lithium-Ion Battery Thermal Management Systems: A Survey and New CFD Results. *Batteries* **2021**, *7*, 86. [CrossRef]
34. Tan, X.; Lyu, P.; Fan, Y.; Rao, J.; Ouyang, K. Numerical investigation of the direct liquid cooling of a fast-charging lithium-ion battery pack in hydrofluoroether. *Appl. Therm. Eng.* **2021**, *196*, 117279. [CrossRef]
35. Yang, W.; Zhou, F.; Zhou, H.; Wang, Q.; Kong, J. Thermal performance of cylindrical lithium-ion battery thermal management system integrated with mini-channel liquid cooling and air cooling. *Appl. Therm. Eng.* **2020**, *175*, 115331. [CrossRef]